



This is a repository copy of *Observations of Running Penumbra Waves emerging in a Sunspot*.

White Rose Research Online URL for this paper:
<http://eprints.whiterose.ac.uk/124474/>

Version: Published Version

Article:

Priya, T.G., Wenda, C., Jiangtao, S. et al. (4 more authors) (2017) Observations of Running Penumbra Waves emerging in a Sunspot. *Astrophysical Journal*, 852 (1). 15. ISSN 0004-637X

<https://doi.org/10.3847/1538-4357/aa9c47>

Reuse

Unless indicated otherwise, fulltext items are protected by copyright with all rights reserved. The copyright exception in section 29 of the Copyright, Designs and Patents Act 1988 allows the making of a single copy solely for the purpose of non-commercial research or private study within the limits of fair dealing. The publisher or other rights-holder may allow further reproduction and re-use of this version - refer to the White Rose Research Online record for this item. Where records identify the publisher as the copyright holder, users can verify any specific terms of use on the publisher's website.

Takedown


If you consider content in White Rose Research Online to be in breach of UK law, please notify us by emailing eprints@whiterose.ac.uk including the URL of the record and the reason for the withdrawal request.



eprints@whiterose.ac.uk
<https://eprints.whiterose.ac.uk/>



Observations of Running Penumbral Waves Emerging in a Sunspot

T. G. Priya^{1,2} , Cao Wenda³, Su Jiangtao^{1,2}, Chen Jie¹, Mao Xinjie^{1,4}, Deng Yuanyong^{1,2}, and Erdélyi Robert^{5,6}

¹Key Laboratory of Solar Activity, National Astronomical Observatories, Chinese Academy of Sciences, Beijing 100012, China

²School of Astronomy and Space Sciences, University of Chinese Academy of Sciences 19 A Yuquan Road, Shijingshan District, Beijing 100049, China

³Big Bear Solar Observatory, 40386 North Shore Lane, Big Bear City, CA 92314, USA

⁴Beijing Normal University No. 19, XinJieKouWai Street, Beijing 100875, China

⁵Solar Physics and Space Plasma Research Centre, School of Mathematics and Statistics, University of Sheffield, Hicks Building, Hounsfield Road, P.O. Box 32, Sheffield S3 7RH, UK

⁶Department of Astronomy, Eötvös Loránd University, Pázmány P. sétány 1/A, Budapest, H-1518, Hungary

Received 2017 August 23; revised 2017 November 17; accepted 2017 November 17; published 2017 December 28

Abstract

We present results from the investigation of 5 minute umbral oscillations in a single-polarity sunspot of active region NOAA 12132. The spectra of TiO, H α , and 304 Å are used for corresponding atmospheric heights from the photosphere to lower corona. Power spectrum analysis at the formation height of H α –0.6 Å to the H α center resulted in the detection of 5 minute oscillation signals in intensity interpreted as running waves outside the umbral center, mostly with vertical magnetic field inclination $>15^\circ$. A phase-speed filter is used to extract the running wave signals with speed $v_{\text{ph}} > 4 \text{ km s}^{-1}$, from the time series of H α –0.4 Å images, and found twenty-four 3 minute umbral oscillatory events in a duration of one hour. Interestingly, the initial emergence of the 3 minute umbral oscillatory events are noticed closer to or at umbral boundaries. These 3 minute umbral oscillatory events are observed for the first time as propagating from a fraction of preceding running penumbral waves (RPWs). These fractional wavefronts rapidly separate from RPWs and move toward the umbral center, wherein they expand radially outwards suggesting the beginning of a new umbral oscillatory event. We found that most of these umbral oscillatory events develop further into RPWs. We speculate that the waveguides of running waves are twisted in spiral structures and hence the wavefronts are first seen at high latitudes of umbral boundaries and later at lower latitudes of the umbral center.

Key words: Sun: chromosphere – magnetic fields – sunspots

Supporting material: tar.gz file

1. Introduction

The first observational evidence of running penumbral waves (RPWs) came from Giovanelli (1972) and Zirin & Stein (1972), who detected concentric intensity waves propagating outward through the penumbra of a sunspot in H α and having azimuthal extents of 90° – 180° and sometimes 360° . These waves, considered to be magnetoacoustic modes, were observed to propagate with a phase velocity of 10 – 20 km s^{-1} and exhibited intensity fluctuations in the range of 10%–20%. Briskin & Zirin (1997) and Kobanov & Makarchik (2004) have revealed how the frequencies and phase speeds of RPWs vary from 3 mHz, 40 km s^{-1} to 1 mHz, 10 km s^{-1} from the inner penumbral boundary to the outer penumbral edge, and becomes gradually invisible while approaching the outer boundary of the penumbra. Additionally, Kobanov (2000) has observed the propagation of RPWs in the chromosphere up to $\sim 15''$ ($\sim 10,000 \text{ km}$) from the outer edge of the penumbral boundary, suggesting the quiet-Sun p -mode oscillations dominate at greater distances, hence overpowering the signatures of any remaining RPWs.

The origin of RPWs has been under debate over years since their discovery, with current research attempting to address whether they are trans-sunspot waves of purely chromospheric origin (e.g., Tziotziou et al. 2006, 2007 and references therein) or the chromospheric signature of upwardly propagating p -mode waves (Christopoulou et al. 2000, 2001; Georgakilas et al. 2000; Centeno et al. 2006). Zhao et al. (2016) have acknowledged that the coupling and interaction of the p -mode waves with the magnetized plasma can possibly cause the running waves. More recently, it has been suggested that RPWs are slow low- β waves

propagating upwards along inclined magnetic field lines (Bogdan & Judge 2006; Bloomfield et al. 2007; Jess et al. 2013; Madsen et al. 2015), facilitating the propagation of non-thermal energy into the corona. Some studies (Alissandrakis et al. 1992, 1998; Tsiropoula et al. 1996, 2000; Rouppe van der Voort et al. 2003) show that they are waves originating from oscillating elements inside the umbra. According to some studies, RPWs and umbral oscillatory events belong to the same traveling wave system and it is likely that the underlying driving physical mechanisms are the same. Lites et al. (1998) proposed that either the RPWs are driven by the umbral oscillatory events or they share a common physical basis. The problem is that an indisputable physical model is not available that could attribute these two phenomena to the same driving mechanism and also explain their differences (periods of 3 and 5 minutes).

On the other hand, there is also evidence that umbral oscillatory events of the chromosphere are not the source of RPWs (Giovanelli 1972; Moore & Tang 1975; Christopoulou et al. 2000, 2001; Tziotziou et al. 2002; Kobanov & Makarchik 2004; Bloomfield et al. 2007). For example, Christopoulou et al. (2001) reported that RPWs are more closely associated with photospheric umbral oscillations than the chromospheric ones. Freij et al. (2014) observed RPWs within a solar pore and interpreted them as upwardly propagating waves (UPWs). They found that the power enhanced at the boundary of the pore at about 3–5 minute, whereas in the chromosphere where the UPWs are observed, the power was reduced. Moreover, Kobanov & Makarchik (2004) found that in most cases the running umbral waves

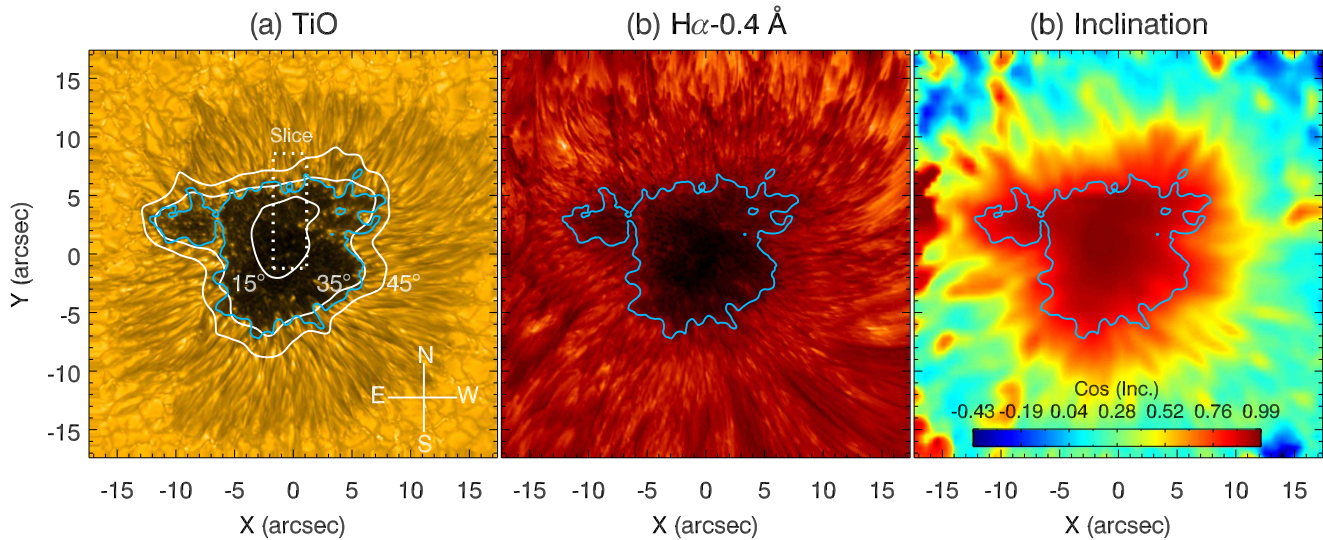


Figure 1. Maps of the leading sunspot in active region NOAA 12132 on 2014 August 5. (a) A TiO image in which a rectangle region marked by dotted lines is selected to be analyzed later. White contours represent the inclinations of 15° , 35° , and 45° and blue contour in (a)–(c) denotes the umbral boundaries (45% of the maximum intensity). (b) A $H\alpha - 0.4 \text{ \AA}$ image. (c) A field inclination image.

terminate rather abruptly at the umbral boundary and show no direct linkage with RPWs. That means not all 3 minute wavefronts can be traced out from the umbra into penumbra. However, the question is where do the RPWs initially emerge in chromosphere: is it from the inner umbra or the umbral boundary of sunspots? Furthermore, how are they linked with umbral oscillatory events—this remains an open question. Here, we present the first observations of RPWs linked to previously occurring RPWs and their further development into new RPWs. We discuss, here, the study of the origin of emergence of RPWs from sunspots using the spectra of TiO, $H\alpha$, and 304 \AA for various atmospheric heights from the photosphere to lower corona. By employing a time series analysis of imaging observations, we track umbral oscillatory events and their association with the preceding and following RPWs. The paper is organized as follows. Section 2 details the observations and reduction of the data presented, Section 3 describes the analysis of the data and studies the umbral oscillatory events at different heights, and Section 4 summarizes and concludes.

2. Observations and Data Processing

High-resolution observations were carried out of the leading sunspot of active region NOAA 12132, on 2014 August 5, from New Solar Telescope (NST, Cao et al. 2010) operating at the Big Bear Solar Observatory (BBSO). We have employed the data set already investigated by Su et al. (2016) to study the spiral structures of wavefronts in the sunspot. The sunspot of our observation is located at S09E08 as shown in Figure 1(a). Observations began at 18:19 UT for a duration of 60 minutes. We used the broadband filter imager of NST, with a field of view (FOV) of $70''$ at the $0''.034 \text{ pixel}^{-1}$ image scale to acquire continuum photospheric images every 15 s in TiO band (705.7 nm , 10 \AA bandpass). We also employed the Visible Imaging Spectrometer of NST that has a single Fabry-Pérot etalon to produce a narrow 0.07 \AA bandpass over a $70''$ circular FOV at $0''.034 \text{ pixel}^{-1}$ image scale. The chromospheric images were thus acquired every 23 s by scanning the $H\alpha$ spectral line from its blue wing -1 \AA to red wing $+1 \text{ \AA}$ with a step size of

0.2 \AA . In addition, we also acquired the simultaneous space observations taken in 304 \AA line (formed in the transition and lower corona) of the Atmospheric Imaging Assembly on the *Solar Dynamics Observatory* (SDO/AIA; Lemen et al. 2012). We chose the first $H\alpha - 1.0 \text{ \AA}$ image as a reference image to align all other images in this passband. The relative shifts were recorded, and used to register the images in the other passbands of $H\alpha$.

Similarly, using the reference image, alignment was easily executed for TiO images and one white-light image at 17:15 UT taken with the Helioseismic and Magnetic Imager (Schou et al. 2012) on board SDO. The aligned white-light image was then used to co-align the 304 \AA images. Finally, Fast Fourier Transform was applied to the time-series images to generate the filtered component images, either in phase speeds of $v_{\text{ph}} > 4 \text{ km s}^{-1}$ (see Su et al. 2016) or centering at certain frequency (e.g., 3.33 mHz, 5.55 mHz, etc.).

3. Analysis and Discussion

3.1. High and Low-frequency Oscillations at Different Heights

In Figure 1(a), we show the map of the sunspot in the TiO image and its corresponding magnetic field inclination map in Figure 1(b) acquired on 2014-08-05. The magnetic field inclination of different range (15° , 35° , and 45°) is shown by different contours. We use this range of inclination to understand how the strength of oscillation varies from umbral center to umbral boundary.

Figure 2 shows the power maps of 3.8–8.0 minute oscillations for the sunspot in the passbands of TiO, $H\alpha = 1.0, -0.8, -0.6, -0.4, -0.2, 0.0 \text{ \AA}$ and 304 \AA , respectively. It is clear from Figures 2(a) and (b) that the power is much weaker in the sunspot than in the quiet Sun at the photosphere. However, the power in penumbrae becomes stronger with the increasing height (see Figures 2(c)–(e)). Evidently, even with such high-resolution ($0''.1$) observations, we still cannot confirm the existence of 5 minute oscillations in the chromospheric umbrae (see Figures 2(d)–(g)). Zhao & Chou (2013) suggested that resonant oscillations exist inside the sunspot, primarily inside the sunspot penumbra. In addition to the overall power

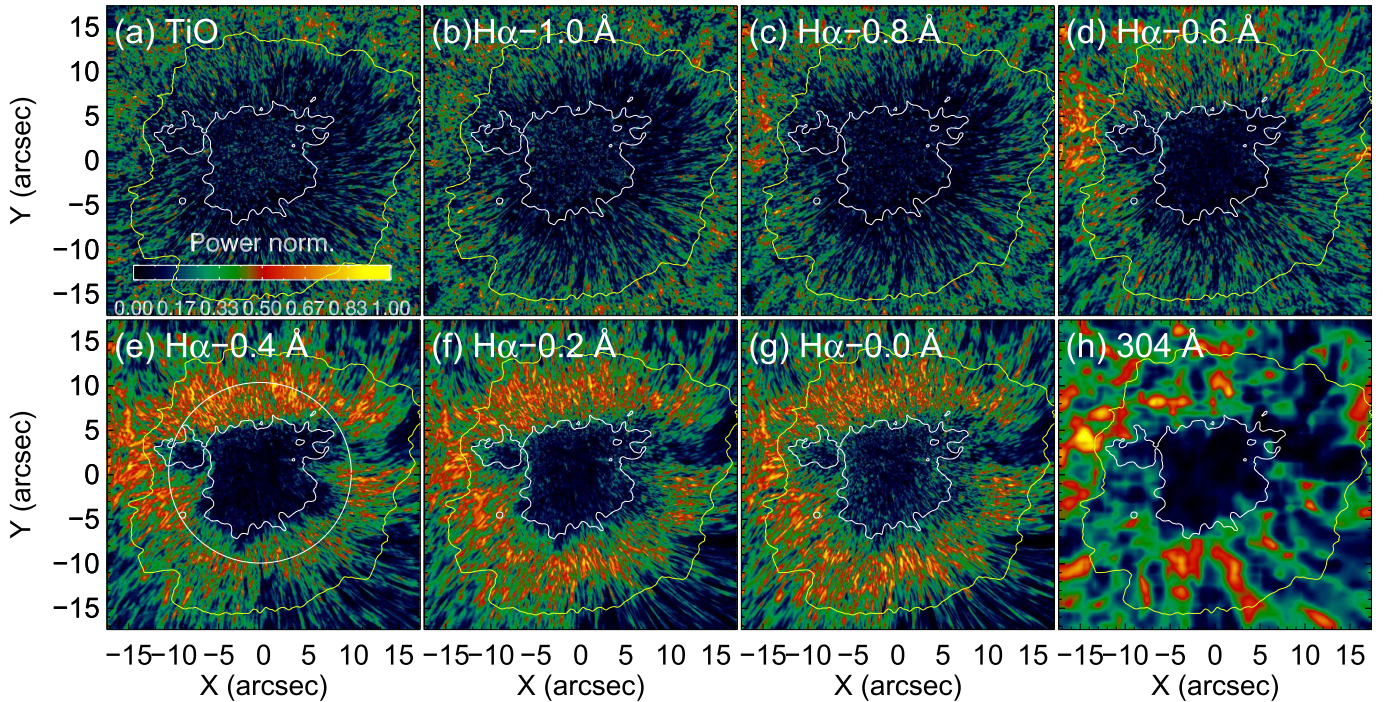


Figure 2. Power maps of the sunspot. (a)–(h) Spatial distribution of the normalized Fourier power for 3.8–8.0 minute oscillations taken in the indicated passband. Umbra regions of sunspots are shown in white contours and penumbral regions in yellow contours (see Figure 1).

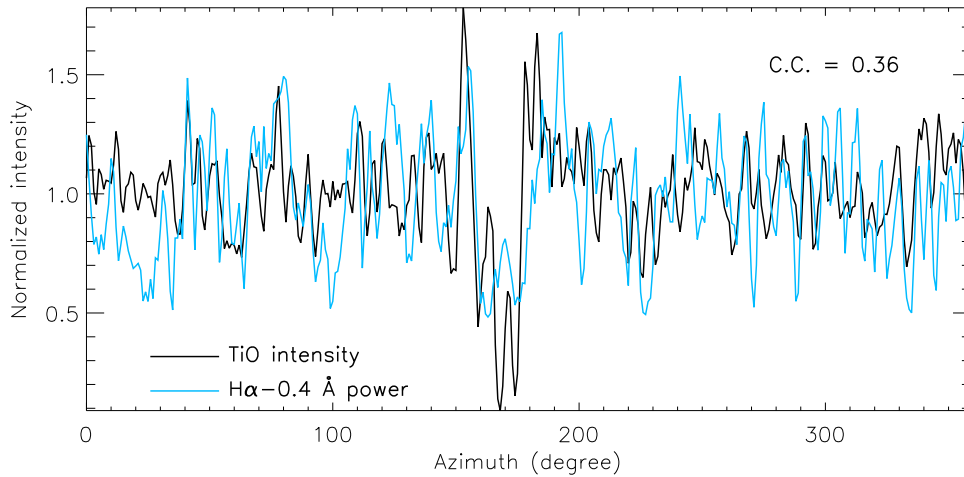


Figure 3. TiO intensity and $H\alpha - 0.4 \text{ \AA}$ oscillation power averaged over the circular slits shown in Figure 2.

enhancement over the penumbra, there are tiny speckles of power scattered everywhere. These tiny speckles are associated much with the bright superpenumbral fibrils. We made a circular slit as shown in Figure 2(e) and plot the intensity curve for TiO and power of $H\alpha - 0.4 \text{ \AA}$, which is shown in Figure 3. It shows that there is probably a slightly higher power concentration in the bright superpenumbral fibrils. We normalized the power spectra by adopting the method of division, wherein each point is divided with the value of maximum intensity in order to compare the power spectra at different wavelengths and positions. The correlation coefficient for the two normalized intensity ≈ 0.36 showing a weak correlation between the intensity and power.

Figure 5 displays the power spectra of oscillations in the sunspot averaged over some circular slits with inclination in the range of the 5° interval between 0° and 35° (e.g., $0^\circ - 5^\circ$, $5^\circ - 10^\circ$, up to $30^\circ - 35^\circ$) in the passband of $H\alpha - 0.4 \text{ \AA}$ (top panel),

and averaged over a circular slit with $0^\circ - 15^\circ$ inclination in the passbands of TiO, $H\alpha - 1.0$, -0.8 , ... and 304 \AA (bottom panel). The noise in the data is removed by performing numerical differentiation on all time series of intensity. We concentrate more on low frequencies, as low frequencies introduce less noise than the high frequencies. In $H\alpha$, beyond the photospheric penumbra, the high-frequency power is almost undetectable while the low-frequency power enhances. We find that most of the power in high-frequency oscillations (period = 1.7–3.8 minute) is concentrated in the umbra (see Figure 4), whereas the power in low-frequency oscillations (period = 3.8–8 minute) is concentrated in the penumbra. We arbitrarily take 3.8 minutes as the cut-off point of 3 minute and 5 minute band oscillations. In Figure 5(a), 5 minute oscillations show their strongest signal appearing in the inclination range of $30^\circ - 35^\circ$, which is close to umbral boundaries (see Figure 1). Subsequently, they decrease while approaching the umbral

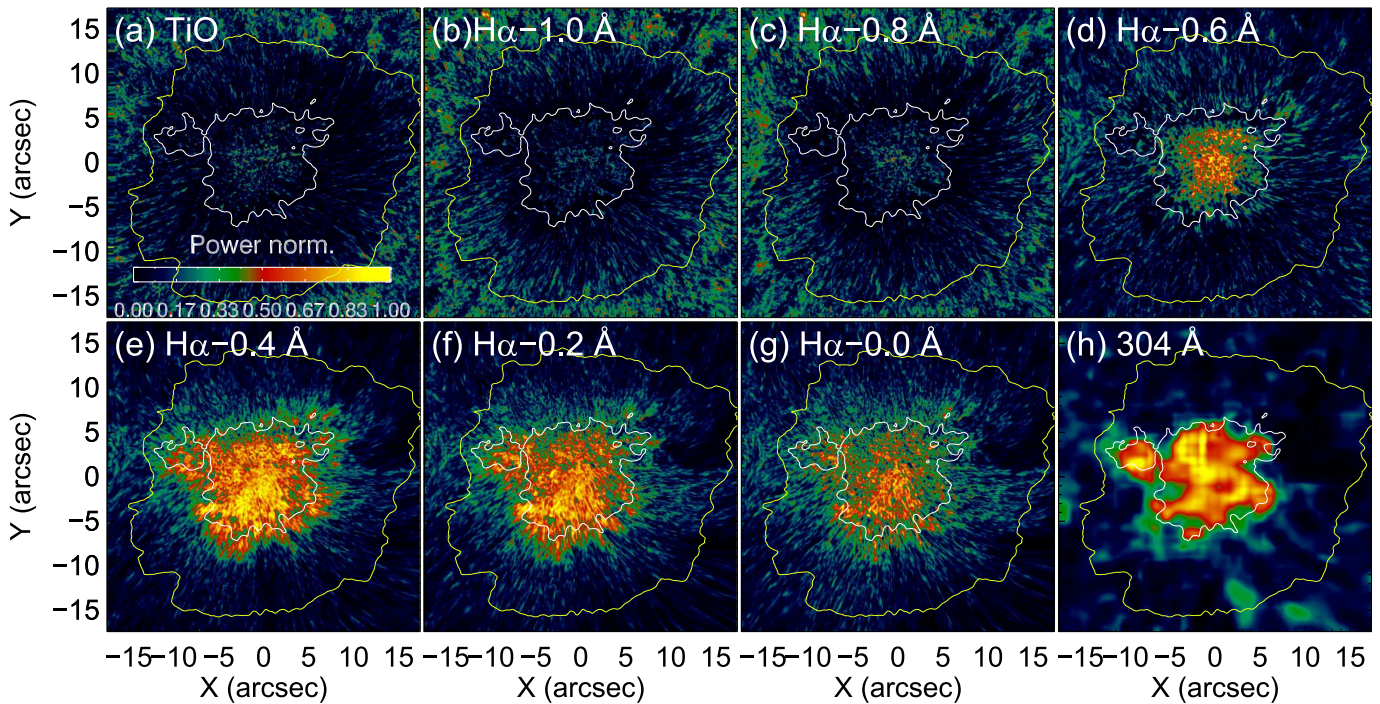


Figure 4. Similar to Figure 2 but for the higher frequency oscillations in a range of 1.7–3.8 minutes.

center and are nearly undetectable in the range of 15° – 20° . Figure 5(b) shows that 5 minute oscillations are stronger at the formation heights of TiO and $H\alpha - 1.0 \text{ \AA}$. However, they become nearly invisible at the formation height of $H\alpha - 0.8 \text{ \AA}$.

We divided the power spectra in Figures 5(a) and (b) into two periodic ranges, $1.7 < P < 3.8$ minutes (short) and $3.8 < P < 8$ minutes (long), and the average power in the two ranges is shown in Figure 6. The variation in power with inclination is plotted in Figure 6(a). For the curve of 3.8–8 minutes, the power increases exponentially with inclination in the range of $\sim 15^\circ$ – 36° . Figure 6(b) demonstrates the variation in power with height. For the 3.8–8 minute curve, it falls off exponentially with increase in height, and fades out while approaching the formation height of $H\alpha - 0.4 \text{ \AA}$. Generally, it is less than 5% for the transmission rate of 5 minute oscillation power from TiO to $H\alpha - 0.4$, -0.2 and 0.0 \AA . Thus, it seems no 5 minute p -mode waves can propagate vertically from photospheric to chromospheric umbra (e.g., within 15° inclination range).

3.2. Time–Distance Diagram for Umbral Oscillatory Events and RPWs

We constructed time–distance diagrams of the Doppler shift (difference of $H\alpha - 0.4 \text{ \AA}$ and $+0.4 \text{ \AA}$), $H\alpha - 0.4 \text{ \AA}$, and AIA 304 \AA as seen in Figure 7, derived for the intensity averaged along a slit of $\sim 3''$ width shown in Figure 1. The connection between the events of umbral oscillations and RPWs are demonstrated in general. In terms of morphology, there is not much difference between panels (a) and (b) and they both show oscillations in umbral regions and wave propagations in penumbral regions. However, they are different from panel (c), which shows the oscillatory features in both umbra and penumbral regions. In the time–distance diagrams, we see a fork pattern forming around the umbral boundary in Figures 7(a) and (b). This pattern is similar to the fork pattern

seen by Chae et al. (2014) but the explanation is quite different. We speculate that the formation of this fork pattern indicates that the umbral oscillatory event emerges close to the umbral boundary and propagates higher up and then a part of the wavefront segregates from the propagating wavefront as it reaches the umbral boundary and moves into the umbral center. This is explained in more detail in the following section. To gather more information, we use a slit and produce two other diagrams in the two time intervals of 18:29:53–18:42:52 UT and 18:43:15–18:56:14 UT, respectively, as shown in Figure 8. In both panels, there are five individual complete umbral oscillatory events, e.g., at 18:31:25 UT, 18:34:05 UT, etc. (named after their kick-off time), but corresponds to four RPWs in panel Figure 8(a) and only three RPWs in panel Figure 8(b), respectively, which might be due to the merging of some of the umbral oscillatory events together or maybe it could not propagate at all. Another puzzling feature is the association of some events of umbral oscillations with their preceding RPWs. For example, events of 18:31:25 UT and 18:34:05 UT were connected to their preceding RPWs by some stripes, which indicates the inward propagation of the associated wavefront toward umbral center. In this paper, we report on 24 events of umbral oscillations in the time interval 18:19–19:19 UT (as shown in Table 1). We then proceed to investigate in detail two of these events by employing time series of imaging observations.

3.3. Imaging Observations of Umbral Oscillatory Events and RPWs

We investigate two typical umbral oscillatory events starting at 18:31:25 UT in panel (e) of Figure 9 and at 18:51:39 UT in panel (d) of Figure 10, respectively. For the first event, the three dark patches, A, B, and C, highlighted by red squares appeared initially close to/on umbral boundaries. It has central field inclinations of $\sim 35^\circ$ (A), 25° (B), and 20° (C) respectively (see Figures 9(b) and (c)). A and B patches separated off from

Power spectrum of differential intensity oscillations

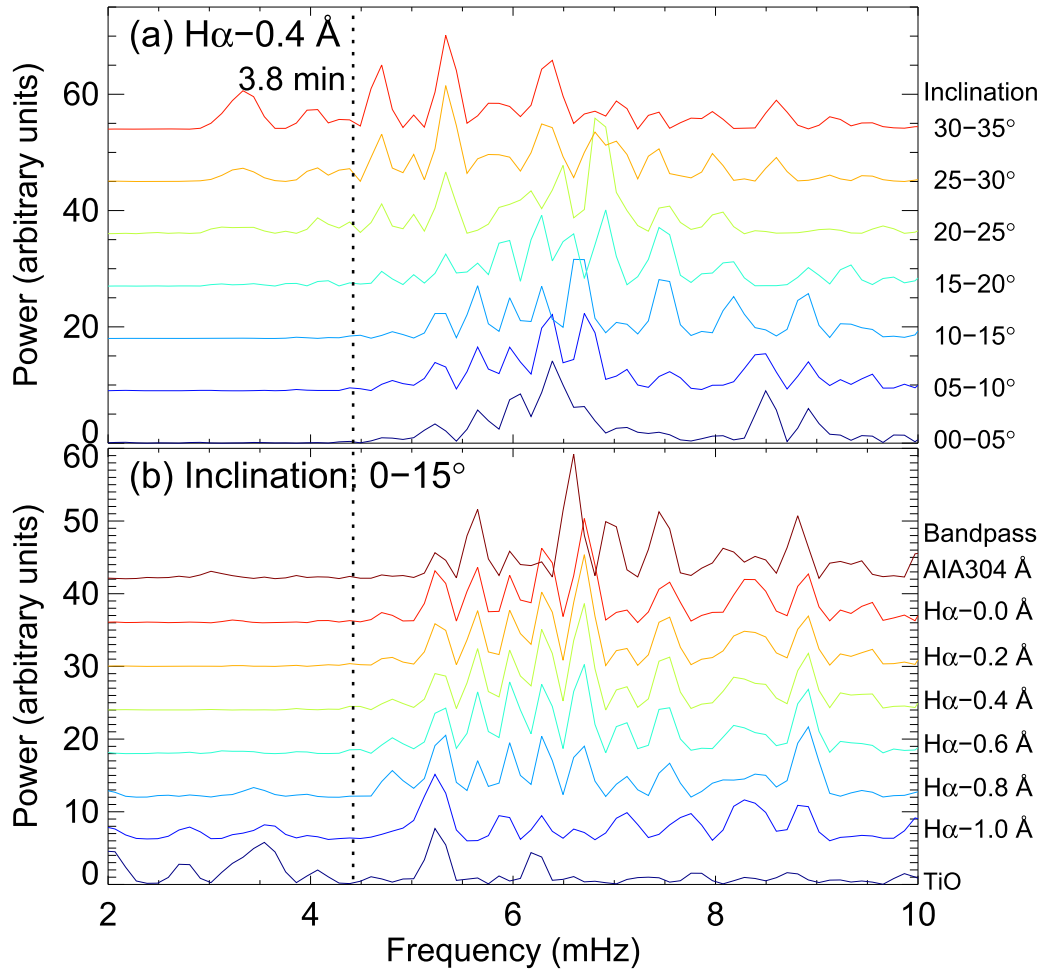


Figure 5. (a) Averaged power as a function of field inclination in the passband of H α - 0.4 Å. (b) Averaged power in a range of 0°-15° as a function of passbands TiO, H α - 1.0 Å, ... and 304 Å.

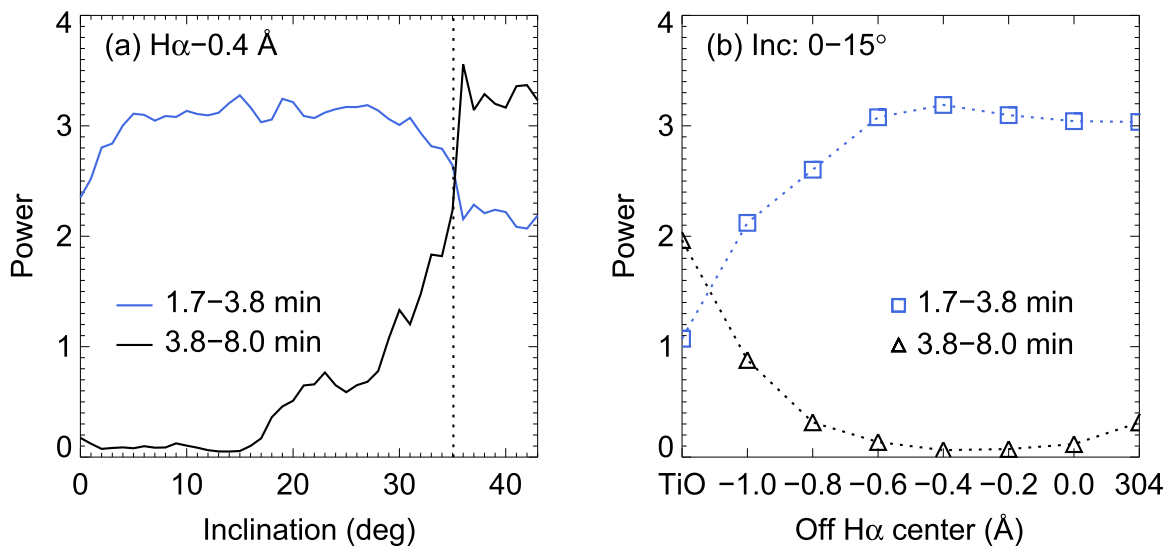


Figure 6. (a) Power spectra of H α - 0.4 Å averaged over a circular slice with an inclination range of 0°-5°, 5°-10°, ... and 30°-35° in the sunspot, where the dotted line gives the limits of the umbra and the penumbra. (b) Spectra of TiO, H α - 1.0, ..., 0.0 Å and 304 Å, averaged over a circular slice with 0°-15° inclination. For better visualization, each curve added with 9 starting from 5° to 0° line in (a) and 6 from H α - 1.0 Å in (b).

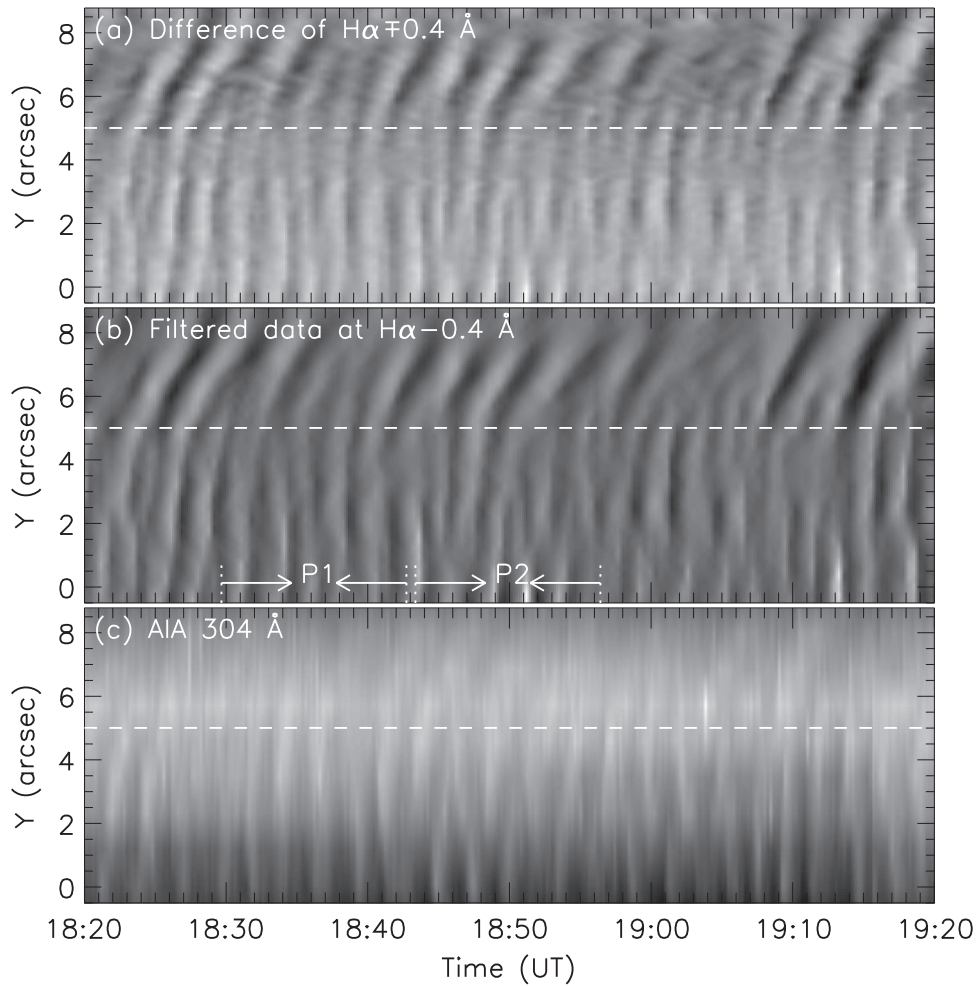


Figure 7. Time–distance diagrams of the Doppler shift (difference of $H\alpha \mp 0.4 \text{ \AA}$), $H\alpha - 0.4 \text{ \AA}$ and AIA 304 \AA , derived for the intensity averaged along the width of the slice shown in Figure 1 for the entire time sequence. The white dashed line marks umbral boundary. The data in (b) marked by the arrows are to be analyzed in the following figure.

the umbral boundaries (see white arrows in panel Figure 9(c)), and patch C stayed where it was. The three patches become enhanced at 18:31:02 UT and then shrink toward the umbral center (see the movie). At 18:31:25 UT, the first event of umbral oscillation began as shown in Figure 8(a).

Later, a dark circular patch formed at 18:31:48 UT in the umbral center and the wavefront began to expand at 18:32:10 UT. In the meantime, the propagation in the clockwise direction at the top takes a spiral form along the trajectory of wavefront (see Figures 9(g)–(i)). In Figure 9(i), the spiral’s top end marked by a red square (denoted as A) separated from its main part and pushed itself toward the umbral center (see the red circles in Figure 9(j)) and a new oscillatory event began again (see Figures 8 and 9). We also notice that the spiral’s tail, which has moved to umbral boundaries, made anticlockwise motions along the boundaries as shown by arrows in Figures 9(h) and (i). At 18:34:05 UT we mark it with a red square (denoted as B) in Figure 9(j) and the next time, it suddenly dived into umbral center to merge with patch A. From then on, the merged patch expanded in the radial direction (see Figures 9(j)–(l)). Also, it is immediately noticeable that the main part of the preceding wavefront crossed the umbral boundaries and became a circular trajectory of RPW.

It is seen in Figure 8 that the stripes are stacked reversely, slightly slanted from 18:33:42 UT to 18:35:14 UT, suggesting

an inward propagation of wavefronts. Figures 9(i) and (j) clearly show the spiral’s top end propagated downward, which provided evident proof for this explanation. It is interesting that the stripes preceding and following the above ones also show this slanted feature.

Similarly, the second event occurring at 18:51:39 UT and in the period of 18:43:15–18:56:14 UT visualized in Figures 8 and 10 showed similar behavior wherein the wavefront propagates toward the umbral center and merges with the preceding wavefront. A part of the merged wavefront jumps into the umbral center forming a new wavefront, which ultimately results in a new umbral oscillation, while the remaining wavefront crosses umbral boundaries to form RPW.

In summary, we have interpreted the developments of features of dark patches A or B in the above five events with the wavefront initially reaching umbral boundaries without showing any further propagation along radial and azimuthal directions. Then, it begins to propagate toward the umbral center the next moment. Hence, it appears to build a connection between the preceding and the following running waves. Some of the major features of umbral oscillatory events and RPWs are summarized in Table 1. It is important to emphasize that the wavefronts in some events were having multi-spiral structures and complicated to determine their initial emergence, whether related to the preceding RPW or not, e.g., event 17 in the table.

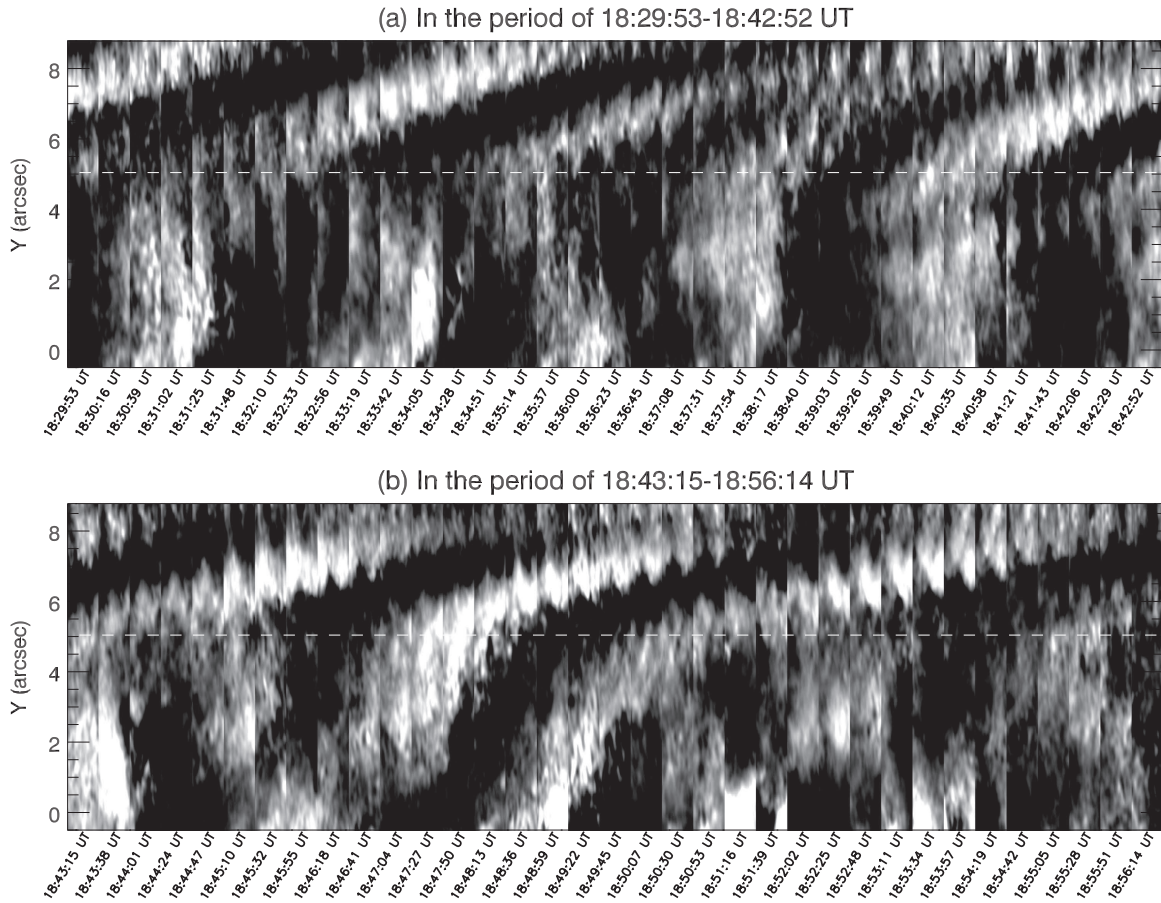


Figure 8. Time–distance diagrams for the slice shown in Figure 1 within the periods of 18:29:53–18:42:52 UT (a) and 18:43:15–18:56:14 UT (b). White dashed line marks umbral boundary.

3.4. Dominant Oscillatory Frequency in the Sunspot Umbra

The distribution of dominant oscillating frequency in the sunspot umbra for event 18:51:39 UT is shown in three phases (see Figures 11(a)–(c)): the initial emergence followed by its propagation toward umbral center and finally its development into RPW. The power of short period oscillation was weak at umbral center, before and after the wavefront propagation (see Figures 11(a)–(b)). Also, one can see that the dominant periods are very much different along the wavefront direction, and the averaged periods over the wavefront edges in the panels are 2.7 ± 5.3 minutes, 2.8 ± 5.9 minutes, and 4.0 ± 7.0 minutes, respectively. This may indicate that the running waves in the sunspot are broadband waves.

3.5. Active Region NOAA 12127

We find similar phenomena occurring in a sunspot of AR NOAA AR 12127. This AR has a complicated morphology due to its light bridges. Figures 12(b)–(d) show power maps of 3.8–8.0 minute oscillations of the sunspots in the passbands of TiO, $H\alpha - 0.4 \text{ \AA}$ and $H\alpha$ -line center. The complicated morphology of the object may impede the revealing of the general regularities and patterns in the observed phenomenon. In spite of this, it is clearly seen in Figure 13 that the wavefront emerged at the center of the umbra, then expanded and rotated clockwise. The wavefront propagates in both azimuthal and radial directions. It takes a spiral form and moves toward the

umbral center and a new oscillatory event begins similar to the events in AR NOAA 12132.

4. Conclusions

We have performed high-resolution imaging observations of active region NOAA AR 12132 to investigate umbral oscillatory events and RPWs. The main results are as follows. The long-period (e.g., 3.8–8.0 minute) oscillations are hardly detectable within the 15° field inclination range in the chromospheric umbra, which is consistent with the theory of MHD waves propagating in a simple, vertically gravitationally stratified atmosphere. The power observed in passbands of $H\alpha - 0.4$, $H\alpha - 0.2$, and $H\alpha$ line center are only 5% of that observed in TiO, suggesting that there is only a 5% transmission rate for 5 minute oscillation power from TiO to $H\alpha - 0.4$, -0.2 , and line center. Moreover, with imaging filtered observations, we find that most of the umbral oscillations initially emerge either at or close to umbral boundaries and also are a part of the preceding RPWs. This new result is also consistent with MHD wave propagation in the inclined magnetic field embedded in gravitationally stratified plasma. These fractional wavefronts are found to be separated from the preceding wavefronts and moves into the umbral center, where they expand radially and begin as new oscillations (an animation showing this phenomena is available online). A closer look at Figure 7(f) reveals that the new wavefront emerges at the umbral center. The panels in

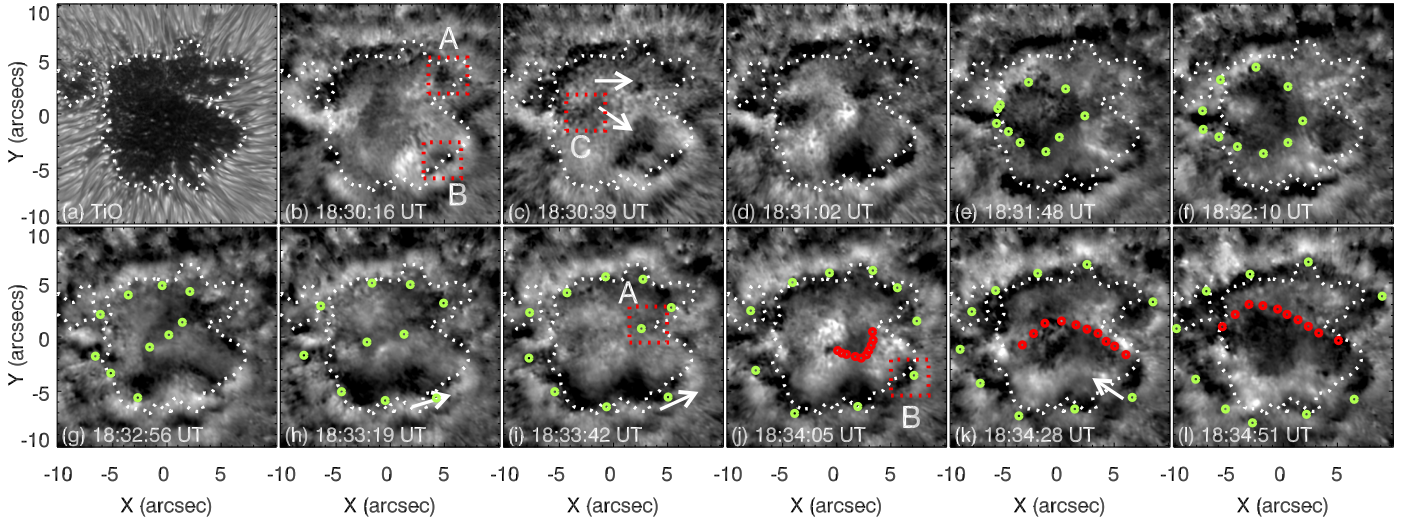


Figure 9. (a) A is a TiO map for reference, and the white dotted contours here and in the other panels mark umbral boundaries. (b)–(l) The time series of filtered $H\alpha - 0.4 \text{ \AA}$ images with phase speeds $>4 \text{ km s}^{-1}$, on which circles are superposed to highlight the trajectories of running wavefronts. Red squares and capital letters A, B, and C mark initial emerging locations of the next umbral oscillatory event. An animated movie is available online.

Table 1
Umbral Oscillatory Events and RPWs in the Period of 18:19–19:19 UT

Umbral Oscillations	Start Time (UT)	θ^a (degree)	$\bar{\theta}$ (degree)	Preceding ^b RPW	Following ^c RPW	\bar{v}^{rpw} (km s^{-1})
01	18:21:24	10°–20°	15°	Yes	Yes	9.8
02	18:23:42	10°–25°	18°	Yes	Yes*	9.8
03	18:25:40	10°–30°	20°	Yes	Yes	9.2
04	18:27:58	15°–25°	20°	Yes	Yes*	9.2
05	18:31:25	40°–30°; 30°–20°; 15°–25°	35°; 25°; 20°	Yes	Yes	10.0
06	18:34:05	15°–30°	23°	Yes	Yes	10.5
07	18:36:23	10°–25°	18°	Yes	Yes*	10.5
08	18:38:17	30°–45°; 10°–30°	38°; 20°	Yes	Yes	13.8
09	18:40:58	15°–30°; 30°–45°	26°; 38°	Yes	Yes	12.8
10	18:44:01	25°–40°; 30°–45°	26°; 38°	Yes	Yes	9.7
11	18:46:18	10°–20°	15°	Yes	Yes	8.0
12	18:49:22	15°–30°	23°	Yes	Yes	7.5
13	18:51:39	10°–20°	15°	Yes	Yes*	7.5
14	18:54:19	0°–15°	8°	?	Yes	10.0
15	18:57:22	25°–40°	33°	Yes	Yes	8.5
16	19:00:26	25°–40°; 10°–25°	33°; 18°	Yes	Yes*	8.5
17	19:03:09	?	?	?	Yes	6.0
18	19:05:50	25°–40°	33°	Yes	Yes	14
19	19:08:08	25°–35°	30°	Yes	Yes	10
20	19:10:03	10°–25°	18°	Yes	Yes*	10
21	19:11:57	10°–30°	20°	Yes	Yes	12
22	19:13:52	0°–35°	18°	Yes	Yes*	12
23	19:16:09	0°–10°	5°	No	Yes	9.0
24	19:19:13	25°–35°	30°	Yes	?	?

Notes. Symbol * denotes the following wavefront catching up and merging with its preceding one.

^a Range of magnetic field inclination at the initial emergence of the umbral oscillatory event.

^b Was the event related to its preceding RPW?

^c Did the event develop into the following RPW?

Figures 7(a)–(e) show that the umbral oscillatory events are related to the preceding RPWs whereas the panels in Figures 7(g)–(l) show that the umbral oscillatory events are related to the following RPWs. In this way, nearly all umbral oscillatory events connect to the earlier occurring RPWs and also develop into new RPWs. This kind of connection between the umbral oscillatory events and RPWs is reported for the first

time through this work. Also, along the wavefront edges, the period of running waves shows a large spread. We finally remark that our new results contribute to observational evidence about how an umbral oscillation is associated with a preceding and following RPWs.

Figures 7 and 9 clearly demonstrates that the wavefronts form a spiral structure, suggesting the waveguides to be twisted (see, e.g.,

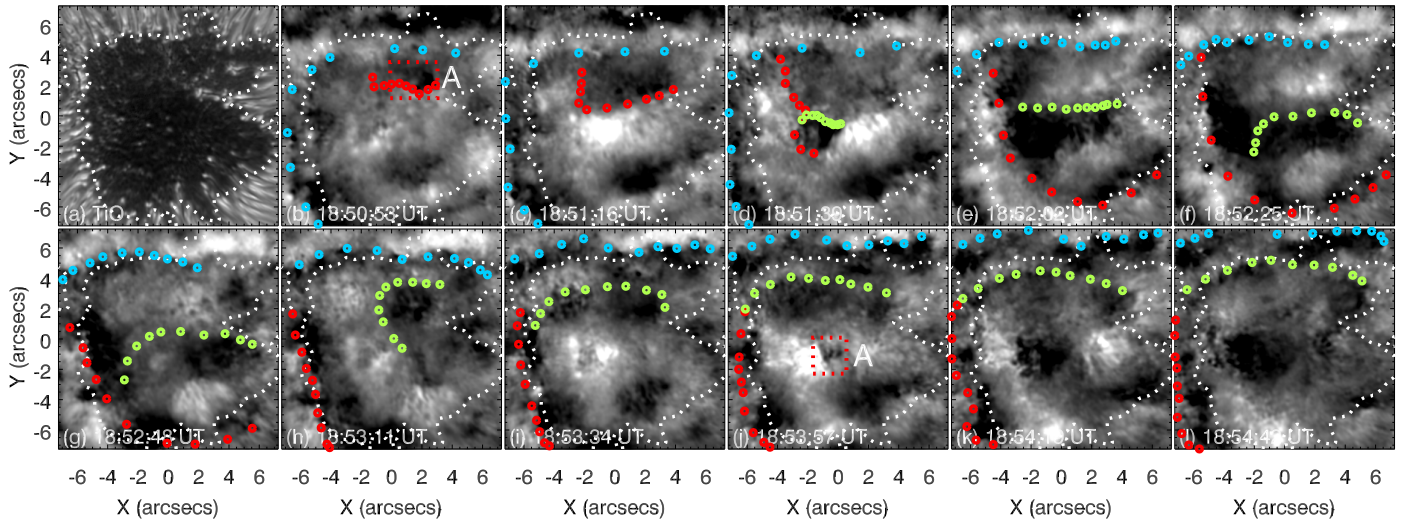


Figure 10. Similar to Figure 9, but for umbral oscillatory events of 18:51:39 UT and 18:53:57 UT.

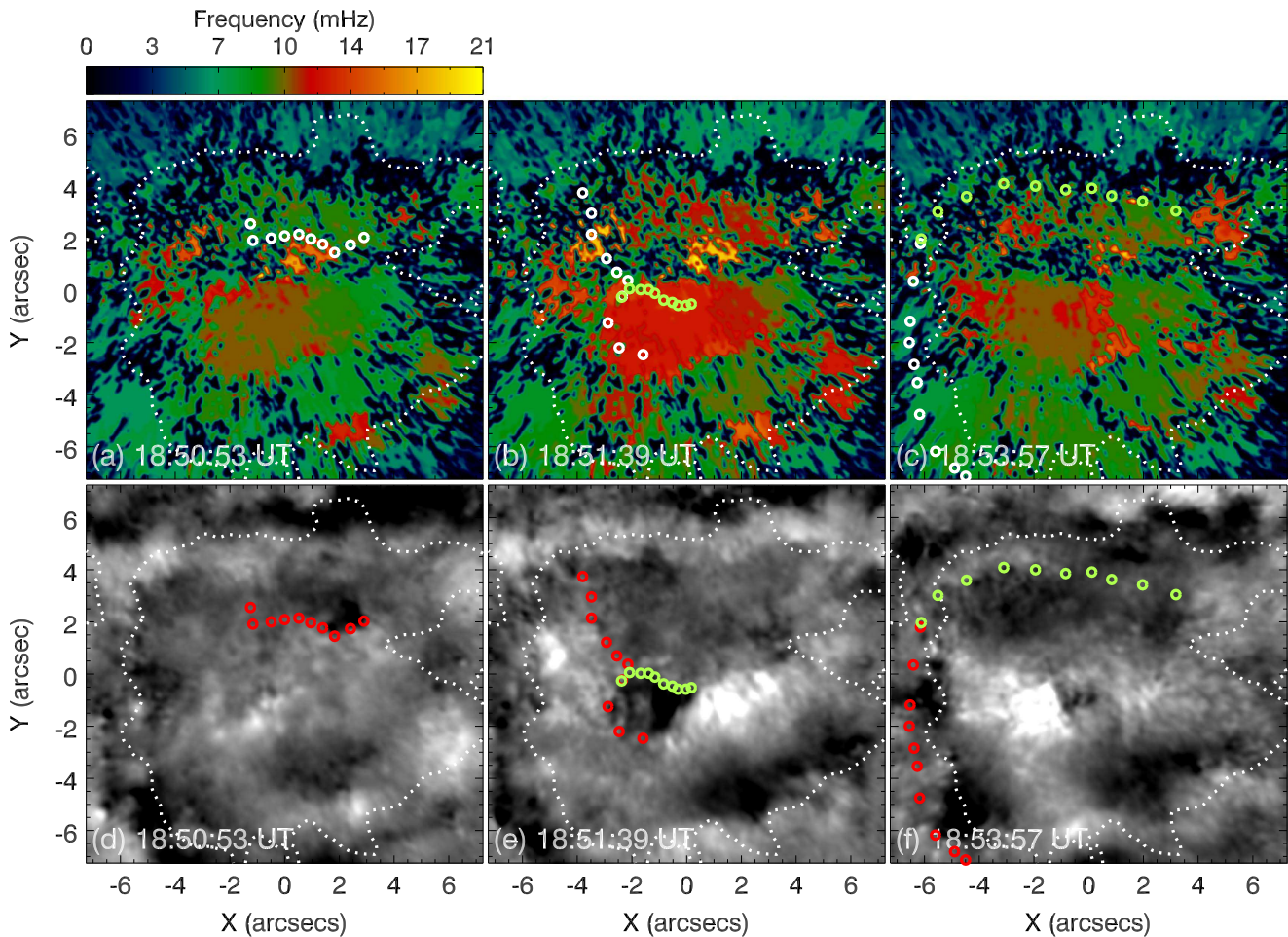


Figure 11. (a)–(c) Distributions of dominant oscillatory frequency in the sunspot umbra, obtained with wavelet analysis for the time series of $H\alpha - 0.4 \text{ \AA}$ filtered images. (d)–(e) The corresponding $H\alpha - 0.4 \text{ \AA}$ filtered images for an event of 18:51:39 UT in the three phases, first emerging, propagating to umbral center and developing into RPW highlighted with circles. White contours in all panels denote umbral boundaries.

Bharti et al. 2010). This observational fact might be the reason why we first see wavefronts at high latitudes and then at lower latitudes at umbral center. However, the problem is still not resolved: RPWs being closely associated with the events of umbral oscillation, but outside the umbral boundaries 5 minute

signals go undetected. It was interpreted earlier that on highly inclined magnetic flux tubes, with the cutoff period increase, magnetoacoustic portals are generated for the propagation of long-period magnetoacoustic waves in the chromosphere, which is also referred to as the leakage of p -modes or photospheric oscillations

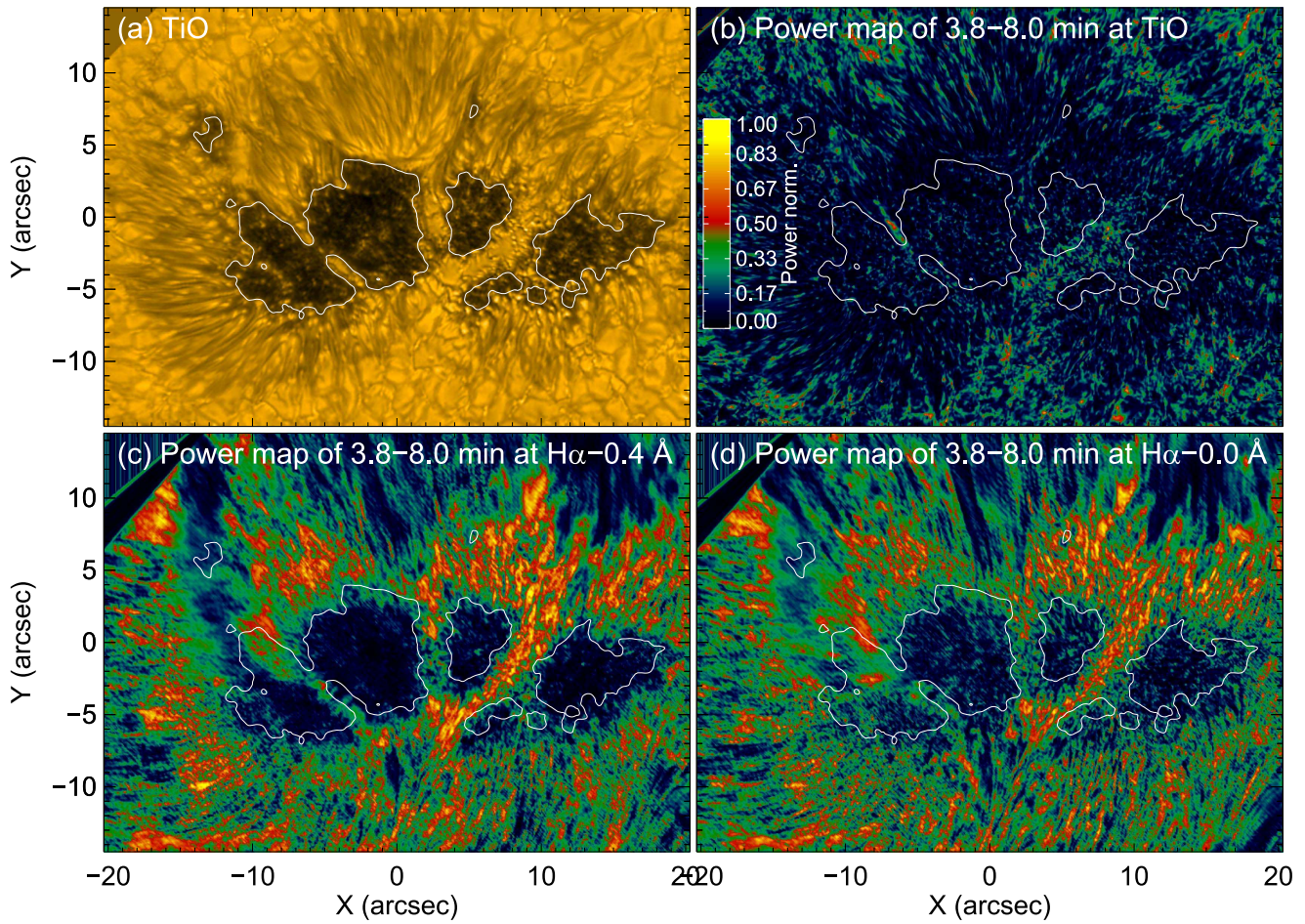


Figure 12. Maps of the main sunspots of AR 12127. (a) The location of sunspots in the TiO image. (b)–(d) Corresponding spatial distribution of normalized Fourier power for 3.8–8.0 minute oscillations taken in the indicated passband. Note that umbral regions of sunspots are shown in white contours.

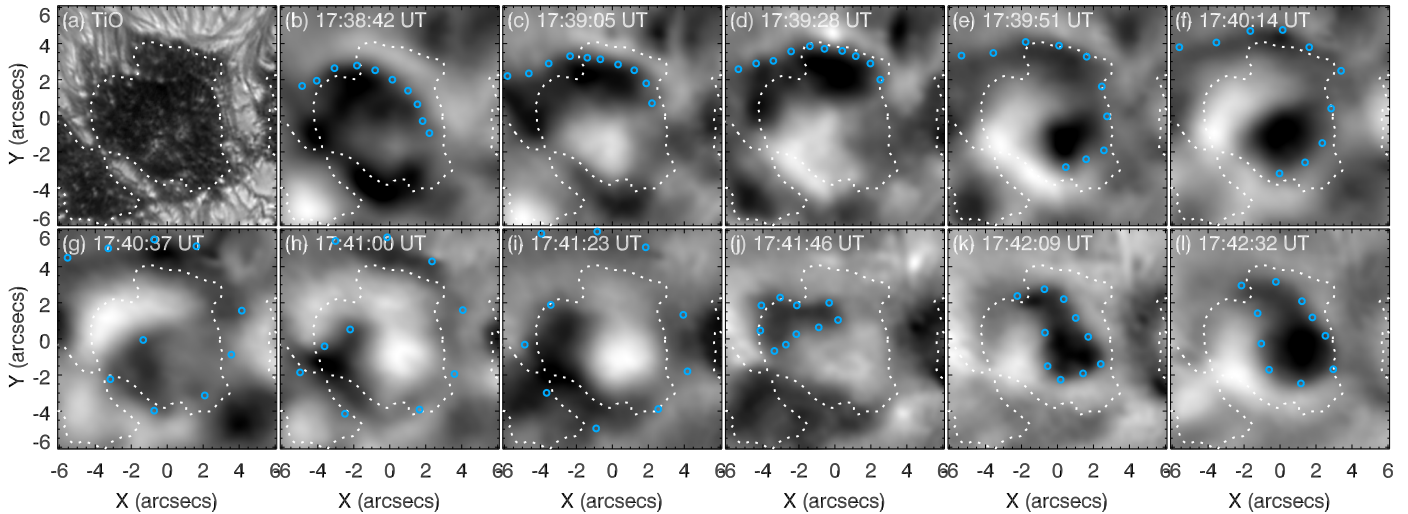


Figure 13. (a) TiO map for reference, and the white dotted contours marks the umbral boundaries. This shows the temporal evolution of the filtered $H\alpha - 0.4 \text{ \AA}$ images with phase speeds $v_{ph} > 4 \text{ km s}^{-1}$. The blue dots show the directions of wave propagation.

(see, e.g., De Pontieu et al. 2004) into the chromosphere. It is worth mentioning that, through MHD simulations, Khomenko et al. (2008) demonstrates that 5 minute oscillations can leak into the chromosphere through small-scale vertical magnetic flux tubes due to the efficiency of energy exchange by radiation in the solar photosphere that can lead to a significant reduction of the cutoff

frequency and may allow the propagation of the 5 minute waves vertically into the chromosphere. We interpret that, to a certain extent, this mechanism strongly supports our observation.

This work is supported by the National Basic Research Program of China under grants 11427901, 11773038,

11373040, 11303052, and 11303048. B.B.S.O. is supported by NJIT, US NSF AGS-1250818, and NASA NNX13AG14G, and N.S.T. is partly supported by the Korea Astronomy and Space Science Institute and Seoul National University, and by strategic priority research program of CAS. T.G.P. would like to acknowledge the financial support from CAS-TWAS Presidents PhD fellowship—2014. R.E. is grateful to the Science and Technology Facilities Council (STFC) UK and The Royal Society, UK. R.E. also acknowledges the support received by the CAS Presidents International Fellowship Initiative, Grant No. 2016VMA045, and the warm hospitality received at NAOC of CAS, Beijing, where part of his contribution was made. We thank referee for the review and for useful comments and suggestions.

ORCID iDs

T. G. Priya  <https://orcid.org/0000-0001-5236-4779>

References

- Alissandrakis, C. E., Georgakilas, A. A., & Dialetis, D. 1992, *SoPh*, **138**, 93
- Alissandrakis, C. E., Tsiropoula, G., & Mein, P. 1998, in ASP Conf. Ser. 155, Three-Dimensional Structure of Solar Active Regions, ed. C. E. Alissandrakis & B. Schmieder (San Francisco, CA: ASP), 49
- Berdugina, S. V., Solanki, S. K., & Frutiger, C. 2003, *A&A*, **412**, 513
- Bharti, L., Solanki, S. K., & Hirzberger, J. 2010, *ApJ*, **722L**, 194B
- Bloomfield, D. S., Lagg, A., & Solanki, S. K. 2007, *ApJ*, **671**, 1005
- Bogdan, T. J., & Judge, P. G. 2006, *RSPTA*, **364**, 313
- Briskin, W. F., & Zirin, H. 1997, *ApJ*, **478**, 814
- Cao, W., Gorceix, N., Coulter, R., et al. 2010, *AN*, **331**, 636
- Centeno, R., Collados, M., & Trujillo Bueno, J. 2006, *ApJ*, **640**, 1153
- Chae, J., Yang, H., Park, H., et al. 2014, *ApJ*, **789**, 108
- Christopoulou, E. B., Georgakilas, A. A., & Koutchmy, S. 2000, *A&A*, **354**, 305
- Christopoulou, E. B., Georgakilas, A. A., & Koutchmy, S. 2001, *A&A*, **375**, 617
- De Pontieu, B., Erdélyi, R., & James, S. P. 2004, *Natur*, **430**, 536
- Freij, N., Scullion, E. N., Nelson, C. J., et al. 2014, *ApJ*, **791**, 61
- Georgakilas, A. A., Christopoulou, E. B., & Koutchmy, S. 2000, *A&A*, **363**, 306
- Giovanelli, R. G. 1972, *SoPh*, **27**, 71
- Home, J. H., & Baliunas, S. L. 1986, *ApJ*, **302**, 757
- Jess, D. B., Reznikova, V. E., Van Doorselaere, T., Keys, P. H., & Mackay, D. H. 2013, *ApJ*, **779**, 168
- Khomenko, E., Centeno, R., Collados, M., & Trujillo Bueno, J. 2008, *ApJL*, **676**, L85
- Kobanov, N. I. 2000, *SoPh*, **196**, 129
- Kobanov, N. I., & Makarchik, D. V. 2004, *A&A*, **424**, 671
- Lemen, J. R., Title, A. M., Akin, D. J., et al. 2012, *SoPh*, **275**, 17
- Lites, B. W., Thomas, J. H., Bogdan, T. J., & Cally, P. S. 1998, *ApJ*, **497**, 464
- Madsen, C. A., Tian, H., & DeLuca, E. E. 2015, *ApJ*, **800**, 129
- Maltby, P., Avrett, E. H., Carlsson, M., et al. 1986, *ApJ*, **306**, 284
- Moore, R. L., & Tang, F. 1975, *SoPh*, **41**, 81
- Roupe van der Voort, L. H. M., Rutten, R. J., Sütterlin, P., Sloover, P. J., & Krijger, J. M. 2003, *A&A*, **403**, 277
- Scargle, J. D. 1982, *ApJ*, **263**, 835
- Schou, J., Scherrer, P. H., Bush, R. I., et al. 2012, *SoPh*, **275**, 229
- Sigwarth, M., & Mattig, W. 1997, *A&A*, **324**, 743
- Su, J. T., Ji, K. F., Cao, W., et al. 2016, *ApJ*, **817**, 117
- Tsiropoula, G., Alissandrakis, C. E., Dialetis, D., & Mein, P. 1996, *SoPh*, **167**, 79
- Tsiropoula, G., Alissandrakis, C. E., & Mein, P. 2000, *A&A*, **355**, 375
- Tziotziou, K., Tsiropoula, G., & Mein, P. 2002, *A&A*, **381**, 279
- Tziotziou, K., Tsiropoula, G., Mein, N., & Mein, P. 2006, *A&A*, **456**, 689
- Tziotziou, K., Tsiropoula, G., Mein, N., & Mein, P. 2007, *A&A*, **463**, 1153
- Wang, T. J., Ofman, L., & Davila, J. M. 2009, *ApJ*, **696**, 1448
- Yuan, D., Nakariakov, V. M., Chorley, N., & Foullon, C. 2011, *A&A*, **533**, A116
- Zhao, J., & Chou, D.-Y. 2013, *SoPh*, **287**, 149
- Zhao, J., Felipe, T., Chen, R., & Khomenko, E. 2016, *ApJL*, **830**, L17
- Zirin, H., & Stein, A. 1972, *ApJL*, **178**, L85